Mechanical Systems and Signal Processing 169 (2022) 108772

Contents lists available at ScienceDirect

Mechanical Systems and Signal Processing

journal homepage: www.elsevier.com/locate/ymssp

In-process detection of cutting forces and cutting temperature signals in cryogenic assisted turning of titanium alloys: An analytical approach and experimental study

Munish Kumar Gupta [a,*], Mehmet Erdi Korkmaz [b], Murat Sarıkaya [c], Grzegorz M. Krolczyk [a], Mustafa Günay [b]

[a] Faculty of Mechanical Engineering, Opole University of Technology, 76 Proszkowska St., 45-758 Opole, Poland
[b] Department of Mechanical Engineering, Karabük University, Karabük, Turkey
[c] Department of Mechanical Engineering, Sinop University, Sinop, Turkey

ARTICLE INFO

Keywords:
Cutting force
Cutting temperature
Finite Element Method (FEM)
Cryogenic cooling
Titanium alloys machining
In-process measurement

ABSTRACT

In-process detection of cutting forces, temperature, roughness, wear etc. during machining of titanium alloys are very important. The Finite element (FE) analysis plays an important role in monitoring and detection of machining responses. It offers a high accuracy in modeling of dry cutting processes and its performance in modeling of cryogenic machining process is a matter of interest. In this context, current investigation focuses on the dry turning and LN_2/CO_2 cooling assisted turning process of commonly used Ti6Al4V alloy. It is very useful material in the biomedical sector, and the simulation of cutting forces and cutting temperature via finite element method (FEM) has been performed. In addition, the simulation results are validated with experimental work. The results show that the deviations between FE modeling and experimental results for the cutting temperature are the average of 5.54%, 5.18% and 8.42% for the dry, LN_2 and CO_2 cooling conditions, respectively. On the other hand, the deviations from FE modeling and cutting force test results were 3.74%, 3.358%, and 3.03% under dry, LN_2 and CO_2 cooling conditions, respectively.

Abbreviations: FEM, Finite Element Method; FE, Finite Element; LN_2/CO_2, Liquid nitrogen and carbon dioxide; F, vector matrix for the force at the element; U, Vector of the determined node displacement; "K", Stiffness matrix; "U", Node displacement vector refreshed with time change; "$M^{1\prime\prime}$, Damping matrix; "$\left\{\dot{U}\right\}$", Node velocity (first derivative of the node displacement); "$M^{2\prime\prime}$, Mass matrix; "$\ddot{U}$", Node acceleration; ALE, Arbitrary Lagrangian-Eularian; σ^0, Flow stress; ε_p, Plastic deformation; $\dot{\varepsilon}^p$, Deformation rate; $\dot{\varepsilon}_0$, Reference plastic deformation rate; T, Workpiece temperature; Tm, Workpiece melting temperature; Tr, Room temperature; A, Yield strength; B, Hardness modulus; C, Strain rate sensitivity coefficient; N, Hardness coefficient; M, Thermal softening coefficient.; P, Hydrostatic pressure; $\overline{\varepsilon}^f$, Fracture strain during the chip separation; D_1, D_2, D_3, D_4, D_5, Fracture constants in JC damage model; JC, Johnson-cook; CVD, Chemical vapour deposition; Q, Heat transfer per unit time; Cv, Specific heat; M, $Mass$; dT/dt, Rate of temperature decrease per unit time, respectively; "q", Heat flux of density; "h", Heat transfer coefficient; T_w, Surface temperature; T_f, Cryogen temperature; Fc, Main cutting force; Ft, Tangential forces; α, Rake angle.

* Corresponding author.
E-mail addresses: munishguptanit@gmail.com (M. Kumar Gupta), merdikorkmaz@karabuk.edu.tr (M.E. Korkmaz), msarikaya@sinop.edu.tr (M. Sarıkaya), G.Krolczyk@po.edu.pl (G.M. Krolczyk), mgunay@karabuk.edu.tr (M. Günay).

https://doi.org/10.1016/j.ymssp.2021.108772
Received 9 September 2021; Received in revised form 6 November 2021; Accepted 19 December 2021
Available online 5 January 2022

1. Introduction

The world of manufacturing especially machining sector is about to endure a seismic shift from conventional to advance processes. With this aim, Industry 4.0 supports the system that enables and reduces the cost of products [1]. Ultimately, obtaining a high quality product cannot be considered as a success alone [2]. However, achieving the most affordable production is among the main goal and expectation in the context of industrial revolution. To reduce the cost of the production process, the optimization of process parameters must be done well [3]. Optimization of machining parameters, cutting tool and cutting conditions reduce the cost [4]. Of course, in addition to all these, it is very common to demand a manufacturing carried out under conditions that may cause the least harm to the environment in the field of manufacturing [5–7].

These days application of sustainable cooling conditions i.e., dry, cryogenics especially with liquid nitrogen and carbon dioxide are used in machining of various materials [8]. These cooling conditions significantly improves the machining performance with less environmental effect [9,10]. Research studies have been carried out to solve the above expectations [11]. But every year, there are technological developments in cutting tools and cutting conditions used in the manufacturing process and machine tools [12,13]. In parallel with these developments, the necessity of continuing the research emerges. To reduce the machining time in the turning process [14], to obtain better quality surfaces [15], to reduce the cost and to minimize the environmental damage of the process [16,17], to improve and develop the cutting tools [18–20] used in turning have gained momentum in recent years. Nath and Kurfess [21] stated that cutting tools with different geometric features such as complex chip breaker form, tip angles of the cutting tip, cutting tool tip radius have been produced and widely used in the industry. However, by considering these geometric features in cutting tools as a whole with cutting parameters, it is necessary to focus on complex problems such as the effect of the chips formed during turning to reduce the damage to the cutting tool and the workpiece by breaking them in appropriate sizes, the workpiece surface quality and the effect on the cutting forces [22] and cutting temperatures [23] during cutting process. Thus, by determining suitable cutting conditions, it is aimed to contribute to obtaine products with minimal cost, time and optimal quality. With this context, there are lot of studies in the literature about finite element modelling of machining process by Papazoglou et al. [24], and especially dry conditions by Akgün and Demir [25]. Zhou et al. [26] predicted the cutting forces in dry turning of Inconel 718 alloy with different tool nose radius and edge radius by finite element simulations. The authors verified the cutting forces by the FE model with the experimental studies in the range of 4% and 11%. Lotfi et al. [27] developed a friction model under 3D dry turning of AISI 304 stainless steel. The researchers verified that the created 3D friction model calculates the friction value depending on the cutting angle and force. Kumar et al. [28] created a 2D FE model to investigate the machinability performance of AISI 1045 steel via nanolayered coated WC-Co cutting insert in dry condition. It was found that the deviation between experimental and predicted force values varied from 1.8 to 3.8% for F_{xz}, which corresponds to the uncoated tool, but the values of coated tool is varied from 1.25 to 6%. Yang et al. [29] compared the surface roughness values obtained by experimentally and FE models in dry turning of Al6061 alloy by PCD cutting tool. They confirm that the good agreement between simulation and experimental responses has been observed, and the FE method can be used to simulate the surface roughness in related studies. Vijayaraghavan et al. [30] performed the FE simulations of dry turning of Inconel718 alloys by data analysis method. The authors verified that the developed FE model is suitable to achieve a goal of sustainable manufacturing. Parida and Maity [31] carried out the hot turning of Inconel 625 alloy experimentally and supported it by FEM. There was a good relation and verification on chip formation and cutting forces between experimental values and FE results. Schindler et al. [32] predicted the thermal influences on Al2024 alloy by FE turning model. The researchers had a good accuracy between experimental and FE results based on the cutting forces and heat flows. Apart from above studies, a brief review about FEM studies for machining of difficult-to-cut materials are given in Table 1.

As can be seen from studies in the literature, the FE studies were generally developed based on dry machining conditions. When cryogenic studies are performed, they are generally experimental, not finite element simulation type [41–45]. To the best of the authors' knowledge, there are no or limited number of FE machining studies based on cryogenic cooling conditions in turning of Ti6Al4V alloys. Considering all these, the machining process is focused on the Ti6Al4V, by subjecting them to dry turning and LN_2 / CO_2 cooling turning process and the simulation of this process with the FEM has been performed. The findings and results are helpful for industrialists using such cooling technologies, and researchers conducting research on these issues. In addition, it has been observed that there are differences between the cooling technologies used in scientific studies and manufacturing industries. All studies examined in this section have shown that the finite element model simulations made by simulation softwares are possible to reach the results compatible with experimental studies.

Table 1
FEM studies for machining of difficult-to-cut materials.

Material	Machining Type	Cutting Tool	Machining Outputs	References
Ti6Al4V	Turning	————	Cutting force, temperature	Sadeghifar et al. [33]
Inconel718	Turning	Carbide	Chip morphology, cutting force, temperature, contact length	Razanica et al. [34]
Ti6Al4V	Turning	Uncoated and TiAlN coated carbide	Chip morphology, cutting force, stress, contact length	Mishra et al. [35]
Inconel718	Turning	Tungsten carbide	Cutting force, temperature, stress	Parida et al. [36]
Ti6Al4V	Turning	Uncoated coated carbide	Chip morphology, cutting force, temperature	Du et al. [37]
Inconel718	Turning	Tungsten carbide	Chip morphology, cutting force, temperature, residual stress	Silva et al. [38]
Ti6Al4V	Turning	TiC coated PCBN	Cutting force, temperature	Veeranaath [39]
Inconel718	Milling	Uncoated ceramic SiAlON	Cutting force and Power	Nieslony et al. [40]

2. Materials and methods

2.1. Finite element method

Finite element analysis is a numerical approximation method that allows complex structures to divided into particles and transformed into idealized structures and mathematically solved [46]. The finite element method includes systematic procedures of derivatives of finite elements that are sub-regions of approximation functions [47]. Numerical solutions for variables at special points are called nodes of each element and are applied to the calculation of finite solutions for the whole geometry [48]. Finite element analysis is useful in providing approaches for solving problems that are analytically difficult or impossible to solve [49]. Discretization of geometry is the first step in finite element analysis, and then the geometry is divided into finite elements. Next, different types of elements are used, such as triangular, quadrilateral, and shallow defined, with the element properties depending on what is required for the analysis. Stiffness matrix is used to define element properties [50]. This matrix expresses the force–displacement relationships of the element under load. Defining the stiffness matrix, the definition of the loading conditions such as pressure, force, and velocity throughout the boundary conditions at the specific node follows. Finally, the expression of the element, the applied loads and the boundary conditions are adapted to the formation of the matrix. The established equations are solved numerically with unknown values. Stress, strain and other properties of interest can be defined depending on the result of the displacement of the node. The equilibrium equations for general linear or nonlinear static problems of finite element analysis can be expressed as Eq. (1) [51].

$$\{F\} = [K]^*\{U\} \tag{1}$$

Here, F is the vector matrix for the force at the element, K is the stiffness matrix and U is the vector of the determined node displacement. However, dynamical analysis requires a different form for dynamical problems independent of time as shown in Eq. (2) [52].

$$\{F(t)\} = [K]\{U\} + [M^1]\left\{\dot{U}\right\} + [M^2]\left\{\ddot{U}\right\} \tag{2}$$

Here "K" refers to the stiffness matrix, "U" to the node displacement vector refreshed with time change, "$M^{1\prime\prime}$ to the damping matrix, "$\left\{\dot{U}\right\}$" to the node velocity (first derivative of the node displacement), "$M^{2\prime\prime}$ to the mass matrix, and "$\ddot{U}$" to the node acceleration (the second derivative of the node displacement). In the formulation of finite elements; Lagrangian, Eularian, and Arbitrary Lagrangian-Eularian mesh structures are widely used. When these mesh structures are compared, it is seen that there are differences between them. In the Eulerian mesh structure, the finite element mesh remains constant during the material flow, only points are displaced. The benefit of the Eulerian mesh structure is that the shape of the elements does not change over time, so there is no distortion or distortion. However, it is imperative to consider the free surface of the chip as the starting shape and the chip formation process cannot be modeled. On the other hand, in the Lagrangian method, there is a movement in the roof. The net is fixed to the material and moves with the net material. However, it is a difficult situation to change the shape of the elements during the material flow. Therefore, the deformed web may need to be regenerated with the mesh. Thus, in the use of such mesh structures; the mesh needs to be re-meshed or adaptive meshing. Also, chip separation criteria are required for shaping chips.

In the Arbitrary Lagrangian-Eularian (ALE) mesh structure, the points on the surface are not fixed neither to the material nor to the area, these points move arbitrarily. In other words, material flow is independent of points. According to Savidis et al. [53], ALE gives better results when compared with both mesh structures. ALE mesh algorithms are used in many softwares used for machining. For instance, it is used in softwares such as ABAQUS, DEFORM, Third Wave AdvantEdge, ANSYS LS-DYNA and gives better results. However, Third Wave AdvantEdge is an only machining simulation software although ABAQUS, DEFORM or LS-DYNA are the simulation softwares about general plastic deformation process. For that reason, Third Wave AdvantEdge was selected as software due to its being of specific FE simulation software that can easy to process. About this issue, Grzesik [54] indicated that the remeshing method used in some of these softwares increases the sensitivity and accuracy of the analysis. Some important boundary conditions are required to use the finite element method for analysis of chip formation in metal cutting. These boundary conditions help to define the limits and loading conditions in order to solve the problem. By applying these boundary conditions, determining the deformation rate of the material, and understanding how the workpiece material will behave during plastic deformation and it is possible to model the chip formation by selecting the appropriate modeling technique and modeling the material. To capture the dynamic behavior of the model, the strain rate and thermal effects of the constitutive equations should be selected. Stress in metals is changed as a function of strain, strain rate and temperature. Johnson-Cook constitutive equation is one of the first equations involving strain and thermal effects according to statement of Xu et al. [55]. Obviously, using these equations, material models such as rigid plastic, elastic–plastic, thermo-elastoplastic, thermo visco-plastic can be created [56]. The formulation of Johnson-Cook's constitutive equation [57] used by Third Wave AdvantEdge is presented in Eq. (3).

$$\sigma^0 = (A + B(\varepsilon^p)^n)\left(1 + Cln\left(\frac{\dot{\varepsilon}^p}{\dot{\varepsilon}_0}\right)\right)\left(1 - \left(\frac{T - T_r}{T_m - T_r}\right)^m\right) \tag{3}$$

Here σ^0 represents flow stress, ε^p plastic deformation, $\dot{\varepsilon}^p$ deformation rate, $\dot{\varepsilon}_0$ refers to reference plastic deformation rate, T workpiece temperature, Tm workpiece melting temperature, Tr room temperature. The coefficient A indicates yield strength (MPa), B hardness modulus (MPa), C strain rate sensitivity coefficient, n hardness coefficient and m indicate thermal softening coefficient.

Moreover, for chip separation situation, a damage model is required. General JC damage model equation for equivalent fracture strain [58] is expressed in Eq. (4).

$$\bar{\varepsilon}^{f} = \left(D_1 + D_2 \exp(D_3 \frac{P}{\bar{\sigma}})\right)\left(1 + D_4 ln\left(\frac{\dot{\bar{\varepsilon}}}{\dot{\bar{\varepsilon}}_0}\right)\right)\left(1 + D_5\left(\frac{T - T_r}{T_m - T_r}\right)\right) \tag{4}$$

In Eq. (4), $\frac{P}{\bar{\sigma}}$ shows the stress triaxiality where P is the hydrostatic pressure that is the average of three-dimensional normal stresses. $\bar{\varepsilon}^{f}$ is the fracture strain during the chip separation which is a dynamic process of machining. The fracture constant of D_1, D_2, D_3, D_4, D_5 in JC damage model equation shows the initial failure strain, exponential factor, triaxial factor, strain rate factor and temperature factor, respectively. The general geometric structure for finite element analysis with Third Wave AdvantEdge is presented in Fig. 1. As the turning method, 3D nose turning shown was preferred.

2.2. Material details

The numerical analysis of machining is directly related to the accurate adaptation of the material model into the software. Therefore, the success of modeling is possible by determining the material properties well and adapting them as input. During the finite element analysis, Ti6Al4V workpiece material having the dimensions of 1x1x3 mm size was selected. The JC parameters and fracture constants previously used by Xu et al. [55], chemical compositions by Gupta et al. [59] and the other mechanical features of Ti6Al4V alloys used by Du et al. [37] in the study are given Tables 2-5, respectively.

The cutting insert was selected as CVD (chemical vapour deposition) type TiC-Al_2O_3-TiN (each assumed as 1 μm thickness [60]) coated carbide inserts with ISO coded of CNMG 120,408 as shown is Fig. 2. The properties of carbide cutting tools previously used by Du et al. [37] are provided in Table 6.

2.3. Cooling systems

Cryogenic is generally defined as the study of low temperature situations [61]. When analyzing a system operating under cryogenic conditions, it should be considered that the thermal features of materials change with temperature. Specific heat, thermal conductivity and especially heat transfer coefficient values for gases and liquids are important thermal properties for heat transfer calculations at cryogenic temperatures. The calculation of heat transfer per unit time (Q) is mentioned in Eq. (5) [62].

$$Q = C_v{}^{*}m^{*}\frac{dT}{dt} \tag{5}$$

In Eq. (5), Cv, m and dT/dt specifies the specific heat, the mass and the rate of temperature decrease per unit time, respectively. By substituting "$m = A^{*}\delta^{*}\rho$" in Eq. (6);

$$Q = C_v{}^{*}A^{*}\delta^{*}\rho^{*}\frac{dT}{dt} \tag{6}$$

The heat flux of density "q" equals to "Q/A". So, Eq. (6) take its the form of Eq. (7) by Newton's heat transfer laws;

$$q = \rho^{*}C_v{}^{*}\delta^{*}\frac{dT}{dt} \tag{7}$$

From Eq. (7), dT/dt is known as the ratio of the temperature differences like the cooling rate $(T2\text{-}T1)/(t2\text{-}t1)$.

$$h = \frac{q}{T_w - T_f} \tag{8}$$

In Eq. (8), "h" is the heat transfer coefficient (W/m^2K), T_w is the surface temperature and T_f *is* the cryogen temperature of LN_2 and CO_2 as −196.5 °C and −78.5 °C, respectively. Moreover, the heat transfer coefficients for LN_2 and CO_2 are adapted as 309 W/m^2K and

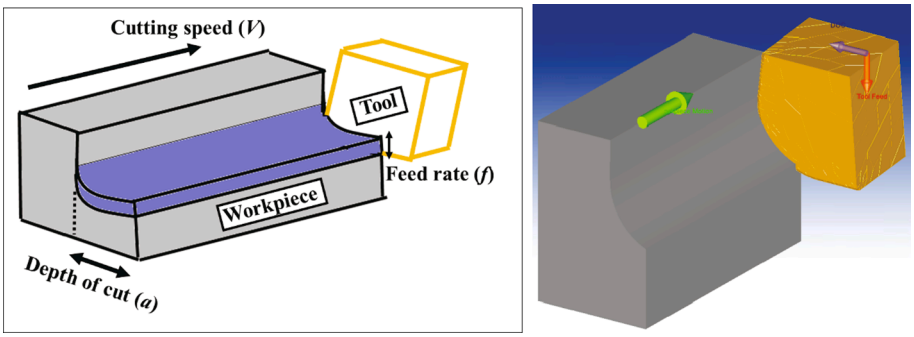

Fig. 1. General geometric structure for finite element (3D nose turning).

Table 2
JC parameters of Ti6Al4V alloys [55]

A(MPa)	B(MPa)	n	C	m
782.7	498.4	0.28	0.028	1

Table 3
JC fracture contents of Ti6Al4V alloys [55]

D1	D2	D3	D4	D5
−0.09	0.25	−0.5	0.014	3.87

Table 4
The chemical content of Ti6Al4V alloys [59]

Ti	Al	V	Fe	C	O
89.9%	5.8%	4.0%	<0.25%	<0.3%	<0.2%

Table 5
The other mechanical and thermal properties of Ti6Al4V alloys [37]

E(GPa)	T_m(°C)	α(10^{-6}/°C)	k(W/mK)	υ	ρ(kg/m^3)	c_p(J/kg°C)
108	1650	9.1	6.8	0.33	4430	526.3

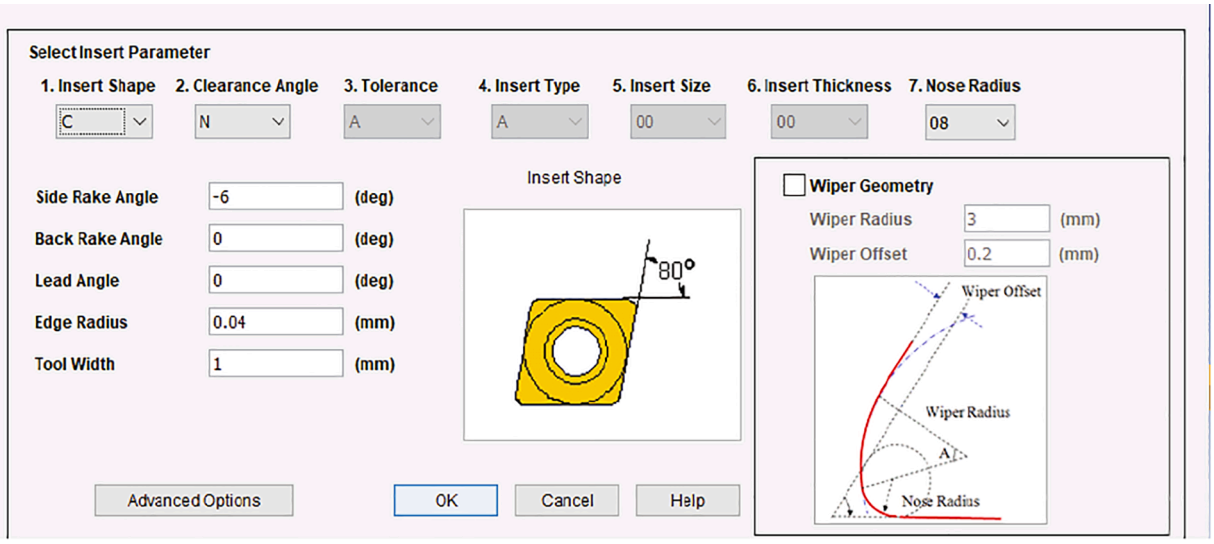

Fig. 2. Tool insert parameters of CNMG 120408.

Table 6
Mechanical and thermal properties of the carbide tool (Copyrights reserved) [37]

E(GPa)	k(W/mK)	α(10^{-6}/°C)	υ	ρ(kg/m^3)	c_p(J/kg°C)
640	50	4.5	0.22	11,900	220

165 W/m^2K [63], respectively as in Fig. 3.

2.4. Meshing

The mesh structure created in the finite element analysis directly affects the analysis results. The main goal is to select a mesh

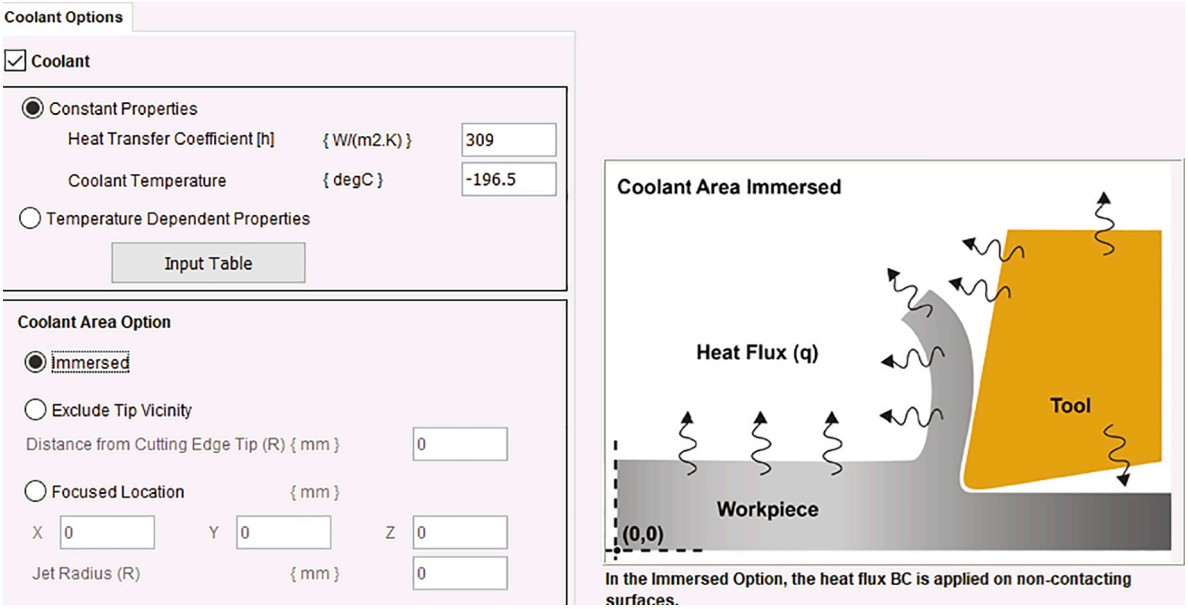

Fig. 3. Cooling options for LN_2 and CO_2 cryogens.

structure that can represent the geometry as much as possible. The density of FEs is an essential measure used to confirm the accuracy of the analysis (element type and morphology also affect the accuracy of the analysis). Assuming the model has no singularity region, the higher density mesh produces outcomes with high precision. Though, the element mesh of the model is very dense and requires a lot of computer memory and long execution time. This drawback often occurs under multiple repeating conditions, especially for nonlinear and transitional analysis. Comparing the findings to test data or theoretical values is one approach to assess the quality of a finite element mesh. Unfortunately, in the early stages of research, test data and theoretical conclusions are frequently unavailable. Therefore, more different tools are required to assess mesh quality. The most important one is the meshing sensitivity analysis. For the current study, the minimum element size for the workpiece and the cutting tool was optimized as 0.15 mm by the mesh sensitivity analysis with re-meshing method shown in Table 7. The simulations were performed with a computer having the RAM of 16 GB, the client cache of 6 GB and the processor speed of 2.4 GHz. All the 8 cores of the computer were used for parallel processing to solve FE analysis faster. It means that 8 FE simulations can be performed at the same time in same solving period. Firstly, the element sizes of 1, 0.5 and 0.25 mm were used in FE analysis and then the results were obtained as 320.1, 298.4, 285.3 N with a computing time of 0.7, 1.5 and 3.3 h, respectively. This showed that the element size should be more decreased due to higher values of change in cutting forces in small computing time differences. Afterwards, the element size was decreased to 0.1 mm step by step. The change in cutting force is so small (ignorable) but the computing time increased about 70%. For that reason, the element size was determined as 0.15 mm (Fig. 4) with a computing time of 6.1 h for a simple test simulation.

2.5. Friction model

In FE simulation of the turning process, Özel [64] suggested that the Coulomb friction model may be quite efficient on the tool flank surface. The average friction coefficient between tool and chip in orthogonal turning was computed from by measuring cutting force as presented in Eq. (9) from a simple turning test for each condition. As a result of the calculation, the average friction coefficient (μ) was found to be 0.46, 0.42, 0.37 for the dry, LN_2 and CO_2 conditions, respectively. In Eq. (9), Fc and Ft are the main cutting and tangential forces obtained experimentally with a dynamometer while α is the rake angle. For instance, average friction coefficient (μ) is calculated as 0.46 when Fc, Ft and α are 270.5 N, 159 N and −6°, respectively. Tangential forces were measured but not recorded in previous study of Gupta et al. [63]

Table 7
The mesh sensitivity analysis for a simple analysis.

Element size (mm)	Cutting force (N)	Simulation solving time (h)
1	320.1	0.7
0.5	298.4	1.5
0.25	285.3	3.3
0.2	276.6	4.8
0.15	**270.5**	**6.1**
0.1	269.5	10.2

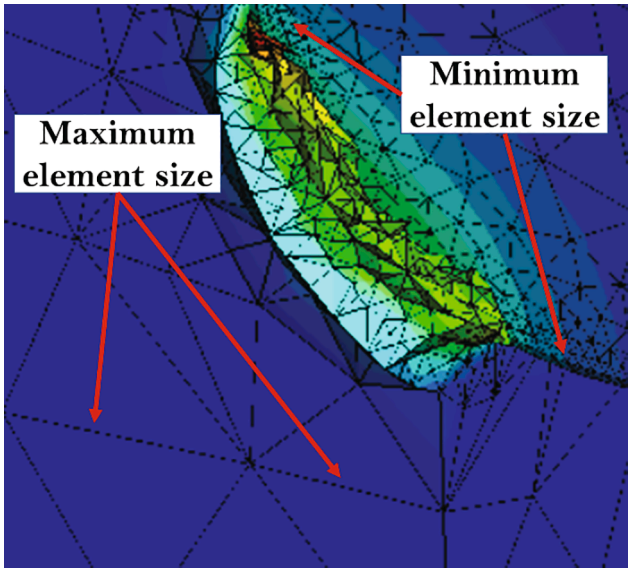

Fig. 4. The minimum element size for a simple test simulation.

$$\mu = \frac{F_t + F_c{}^{*}tan\alpha}{F_c - F_t{}^{*}tan\alpha} \tag{9}$$

3. Experimental procedure for verification

In this work, the same experimental conditions of Gupta et al. [63] were adopted for performing the simulation. The machining of commercially used Ti6Al4V alloy was performed with the CVD type TiCn-Al_2O_3-TiN coated carbide with ISO coded of CNMG 120,408 rhombic shaped inserts. The work piece dimensions were the diameter of 30 mm and the length of 100 mm. The initial layer of 0.5 mm was removed in order to maintain uniformity of workpiece. The side cutting edge angle also known as principle cutting angle used was 90° having 0.8 mm nose radius. Further, the experiments were performed under same conditions with FE simulations. For this purpose, the CNC lathe machine with control system of Siemens were used. The specifications of CNC center and parameters used for cryogenic cooling system by Gupta et al. [63] are given in Table 8.

The levels of the feed rate and the cutting speed under dry, LN_2 and CO_2 were selected based on the previous work of Gupta et al. [63]. As mentioned earlier, the same machining conditions were adopted and the experimental design is shown in Annexure 1. The cutting depth of 0.5 mm and the machining time of 60 s were used throughout the experiments. These parameters were purely selected by following tool manufacturer guide and preliminary studies. The details of machining parameters were listed in Table 9. Then, the cutting temperature and cutting forces were evaluated with the help of Fluke make thermal camera and Kistler made 9257A dynamometer. All these measurements were in online mode and the dynoware package was utilized to extract the cutting forces from the system. The complete process methodology is given in Fig. 5.

4. Results and discussions

4.1. FE simulation results

The simulation study performed with Thirdwave Advantage software using the process parameters and boundary conditions detailed are shown in above sections, 3D turning was analyzed and a new finite element model was developed. Fig. 6 shows a sample test of finite element simulations for the feed rate of 0.1 mm/rev and the cutting speed of 50 m/min.

Table 8
Technical parameters of CNC turning center and cooling conditions [63] (Copyrights reserved).

Machine	Specifications
CNC lathe machine	Minimum and maximum spindle speed 200–3000 RPM with 6KW motor.
Cooling condition details	Flow rate of coolant: 0.35 L / min, pressure: 4 bar, dimensions of nozzle: 1 mm brass nozzle diameter, 2 nozzles with position at rake face

Table 9
The machining factors and their levels [63] (Copyrights reserved).

Factors	Level		
	1	2	3
Cutting speed, V (m/min)	50–75−100		
Feed rate, f (mm/rev)	0.1–0.15–0.2		
Cooling conditions	Dry - LN_2 - CO_2		

4.2. Main cutting forces

In metal cutting processes, cutting force is the force necessary to remove material from a resistive body. The principle cutting force and its parts are affected by a variety of variables. Cutting parameters, workpiece material, cutting tool properties and cutting environment are the most basic factors known to be effective on cutting force according to Yang et al. [65]. Knowing the cutting force is helpful when it comes to sizing the cutting tool, estimating the power required for cutting, optimizing the cutting parameters, etc. Considering all this, as a result, minimal cutting force is often desirable in machining operations. In current section, the influence of cutting parameters and cutting environment on the main cutting force has been determined via finite element analysis and the results are presented graphically in Fig. 7. In parallel with the increasing cutting speed, an increase in cutting force was observed in all three feed rates and cutting environments. For example, when the calculation is made according to each increasing level of cutting speed, the increase in cutting force was between 16.56% and 23.70% at 0.1 mm/rev feed, between 18.24% and 28.17% at 0.15 mm/rev feed, and between 14.23% and 26.36% at 0.20 feed mm/rev. In many previous studies, unlike this study, with increased cutting speed, Pathak et al. [66] and Şeker et al. [67] proved that there is a reduction in cutting force in machining of Al-(1–2) Fe-1 V-1Si alloy and St44 steel, respectively. Ravi and Pradeep Kumar [68] stated that the reason for this situation is the thermal softening effect of the work material because of heat generated by rise in cutting speed in machining of titanium alloys. However, in current work, the force ascends with elevated cutting speed. Generally, when the workpiece materials are subjected to deformation, strain hardening occurs in the material in addition to the thermal softening event. An increase in cutting force can be observed if the strain hardening effect exceeds the thermal softening effect. Therefore, in this study, the rise in force versus cutting speed was associated with strain hardening as a similar observation was also done by Hou et al. [69] and Shi et al. [70]. As can be seen from the Fig. 7, a rise in feed triggered an increase in cutting force. Depending on the rise in feed, the increase in cutting force ranged from 6.72% to 23.11%. However, when compared to the influence of cutting speed, the feed had lower impact on cutting force. This phenomenon may be associated with higher feed rate, which increases the contact area at the tool-chip interface as more material is removed per unit time mentioned by Kim et al. [71]. When Fig. 7 is examined, it can be determined that the cutting environment offering the lowest cutting force in each cutting parameter is LN_2 cooling followed by CO_2 and dry environment. Compared to dry cutting, 21.01% to 34.95% less cutting force can be achieved with LN_2 assisted cutting. In addition, thanks to CO_2 assisted cutting, this improvement can reach up to 14.41%. The improved strength and hardness of the tool material, decreased tool wear, and eliminated adhesion between the tool-chip and tool-workpiece interfaces gained by reducing the cutting temperature may be result in lower cutting forces achieved by LN_2 and CO_2 assisted machining. Since LN_2 has a lower boiling temperature than CO_2, it prevents the cutting tool from overheating during machining and offers more effective cooling ability as thought by Pusavec et al. [72]. Also, Hong et al. [73] indicated that the outstanding performance of LN_2 cooling may be that the liquid/gas buffer across the contact surface absorbs the heat generated and provides a lubricating effect that evaporates quickly and reduces friction.

4.3. Cutting temperature

Cutting temperatures are highly dependent on machining parameters, workpiece material and tool material characteristics. In particular, the characteristics of the material being machined are of vital importance in determining the range of cutting temperatures. For example, Singh et al. [74] demonstrated that titanium alloys, which have much lower thermal conductivity than steels, lead to higher cutting temperatures during machining. Because Ti6Al4V has a limited thermal conductivity, roughly 80% of the heat generated stays in the cutting zone. On the other hand, during the machining of some materials like aluminum, Pramanik [75] declared that more heat is thrown out along with the chips. In the current section, the effect of cutting parameters and cutting environment on the main cutting force has been determined via finite element analysis and the outcomes are provided graphically in Fig. 8. The upward effect of cutting speed on temperature can be noticed from Fig. 8. The degree of this effect varied between 23.61% and 81.25%, depending on the feed rate and cutting environment. In general, a higher cutting speed accelerates the build-up of cutting temperature. It was resulted of more heat produced per unit time and less time available for heat evacuation from the region [76]. Feed rate was found to have a lesser effect on the cutting temperature. That is, the increase in temperature was up to 16.89% in response to an increase in feed from 0.1 to 0.2 mm/rev. This is most likely due to the increased feed causing more friction between the removed material and the cutting tool, which increases the energy in the system and hence raises the cutting temperature. This finding is consistent with prior research of He et al. [77]. With machining under LN_2, the cutting temperature is drastically reduced compared to machining under dry and CO_2 machining. This phenomenon is due to the fact that when LN_2 is injected to the tool-chip contact region, it absorbs heat and evaporates rapidly from area, causing the cutting temperature to drop. LN_2 lowered the temperature from 58.43% to 73.53% compared to dry, and from 40.32% to 57.14% compared to CO_2. Another observation is the slowing down of the LN_2 temperature reduction rate with increasing cutting speed and feed. This is evidence that the cooling efficiency of LN_2 decreases at

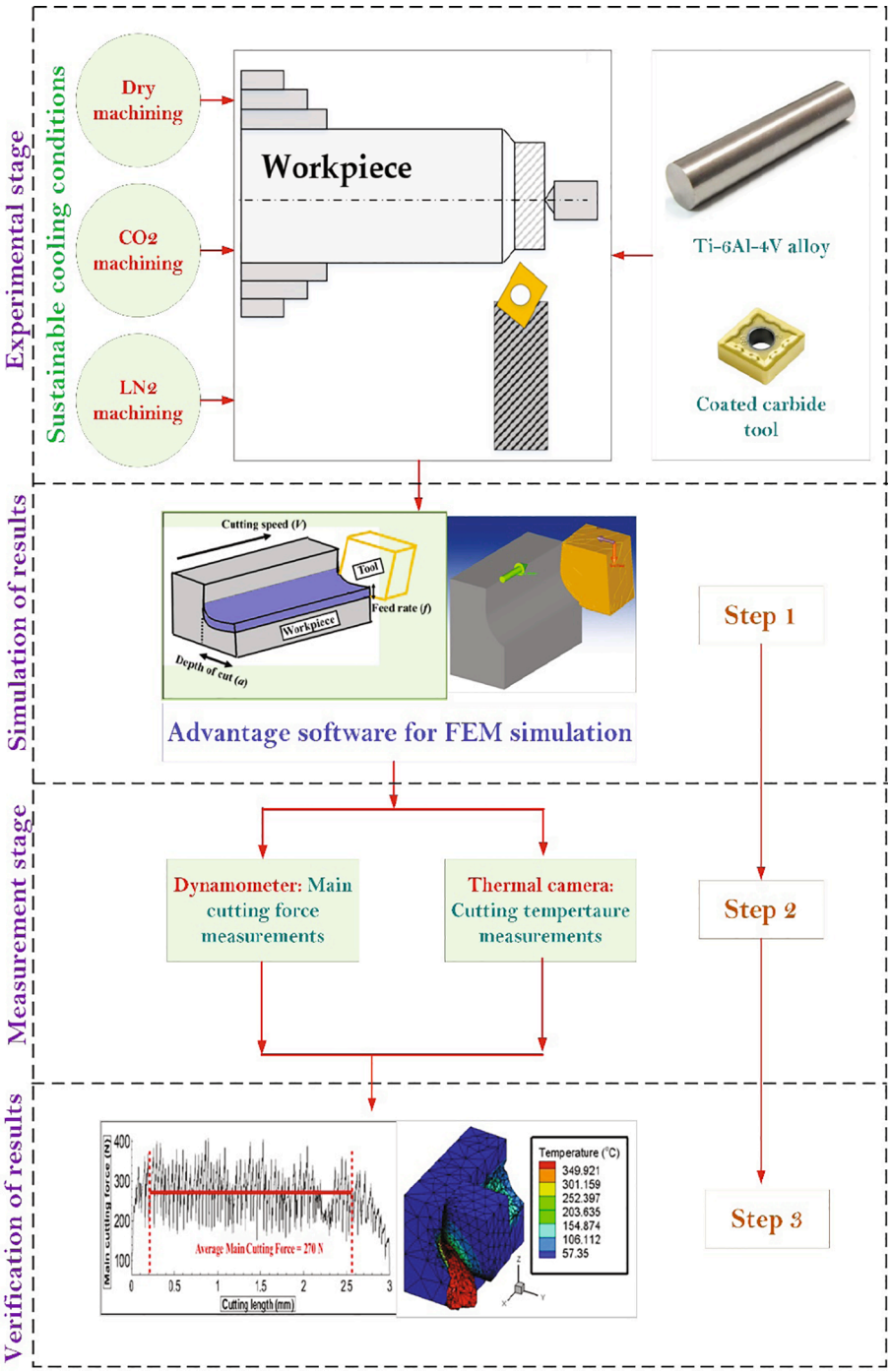

Fig. 5. The complete process methodology.

elevated cutting speeds and feed rates. In addition, since LN_2 has a lower boiling temperature than CO_2, Pusavec et al. [72] stated that it prevents the cutting tool from overheating during machining and offers more effective cooling ability.

Moreover, to verify the data in Fig. 8, the steps of a simple finite element simulation for the evaluation of the maximum cutting temperature are given in Figs. 9, 10 and 11 for the dry condition, LN_2 and CO_2 cooling conditions, respectively.

As shown in Figs. 9-11, there is a maximum temperature on the contact surface of the cutting tool. For this reason, the heat generated between the tool and the chip affects the performance of the tool and the surface quality of the machined workpiece. The friction that occurs in the slip zone also affects the mechanical properties of the machined material and causes tool wear, and higher cutting forces due to the heat generated in the tool, chip-tool and workpiece contact area. Moreover, the relation between cutting

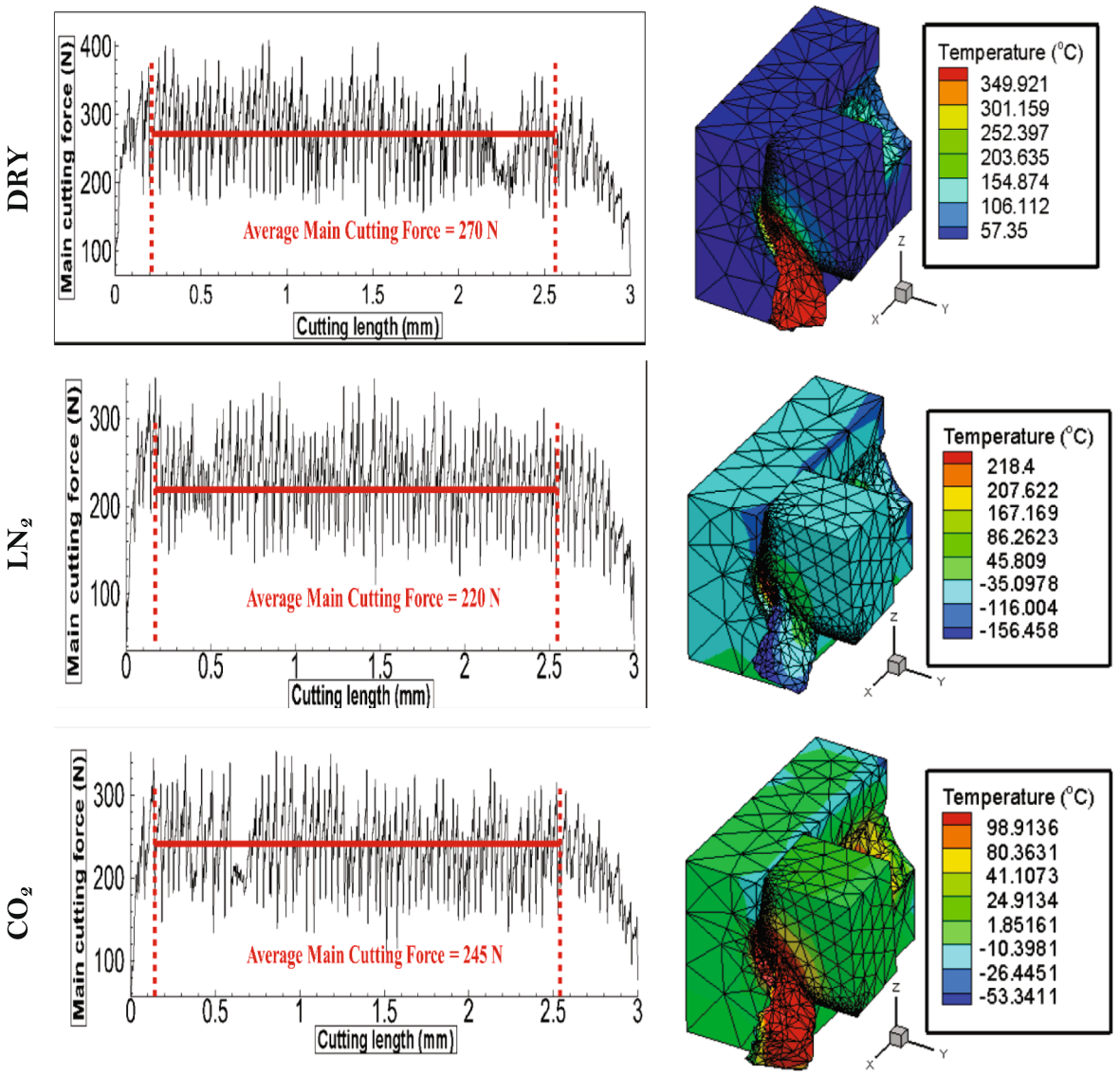

Fig. 6. Sample finite element simulations for the feed rate of 0.1 mm/rev and the cutting speed of 50 m/min.

forces and cutting temperature well explained in Fig. 12.

4.4. Verification of FE analysis results by turning experiments

In Fig. 12, the comparison of the cutting temperature and cutting forces obtained as a consequence of the experimental study and FE analysis shown graphically. The results obtained are very close to each other and the curves obtained from the graph quite consistent with each other. This phenomenon shows that the experimental results verified the FE model results in high accuracy.

Based on Fig. 12a-c-e, the deviations between FEM and experimental results for the cutting temperature are the average of 5.54%, 5.18% and 8.42% for the dry, LN_2 and CO_2 cooling conditions, respectively. On the other hand, the deviations from FEM and cutting force test results in Fig. 12b-d-f averaged 3.74%, 3.35%, and 3.03% under dry, LN_2 and CO_2 cooling conditions, respectively. In the literature, most of the FE machining studies shows that the deviation less than about 10% is thought as the acceptable range between the finite element model results and experimental validation as mentioned before by Özel et al. [78]. After the verification of the FE model, the possible wear region of the cutting inserts was evaluated for each cutting conditions. Fig. 13 shows the possible wear region of the inserts evaluated by FE model and the actual wear region of the cutting inserts after experimental turning previously used by Gupta et al. [63]. The experimental and FE images of the cutting inserts are also so similar with respect to tool wear, and this phenomena also verified the FE model which is developed for the cryogenic turning process of Ti6Al4V alloy.

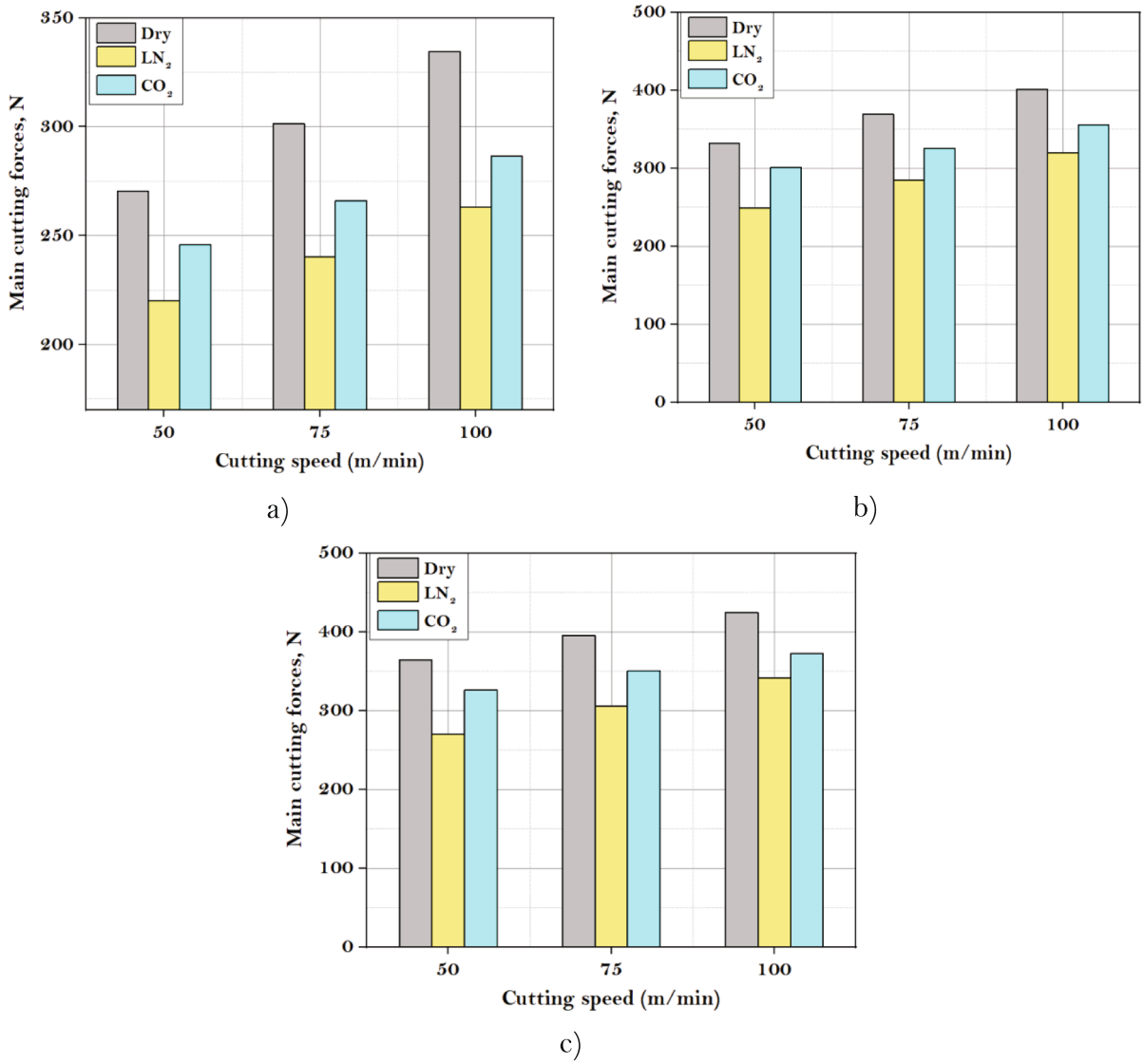

Fig. 7. Finite element results for the main cutting force at the feed rate of a) 0.1 mm/rev, b) 0.15 mm/rev, c) 0.2 mm/rev.

5. Comparison of the results

The most common reason about the deviations between the FE model and experimental results are the meshing accuracy and friction model since these parameters are just assumed in the FE model. The other possible reason for this is considered to be that the Johnson Cook parameters adapted for the workpiece material model are obtained from the literature. However, the mechanical properties of the workpiece material used in the present study may have different from the same materials in the literature due to different microstructures caused by different manufacturing methods or heat treatments as thought by Guo et al. [79]. Mechanical properties are mainly due to interatomic bond strengths. However, the internal structure (microstructure) of the material also has an effect on it. In this way, it becomes possible to obtain different mechanical properties, namely tensile, compressive strength, hardness, toughness in the same material by changing the microstructure. Moreover, there may be different tensile strength values of the same material under the same condition of the tensile tests. For that reason, it is generally taken the average of the 3 ~ 5 tensile strength values from the identical situation of tests [80]. On the other hand, one of the other methods differing the microstructure of the same material is precipitation hardening. Abdel-Salam et al. [81] defined the precipitation hardening as to ensure that the second phase, which is present in less amount in the material and it is precipitated in the form of particles in the main phase, thereby increasing the strength of the material. According to Fu et al. [82], this method is one of the most important methods used to increase the strength of materials and is generally used in non-ferrous metal alloys (Al, Ti, Mg). The main reason for the increase in strength in the precipitation hardening process is explained by the limitation of the dislocation movements of the precipitates formed as a result of the precipitation

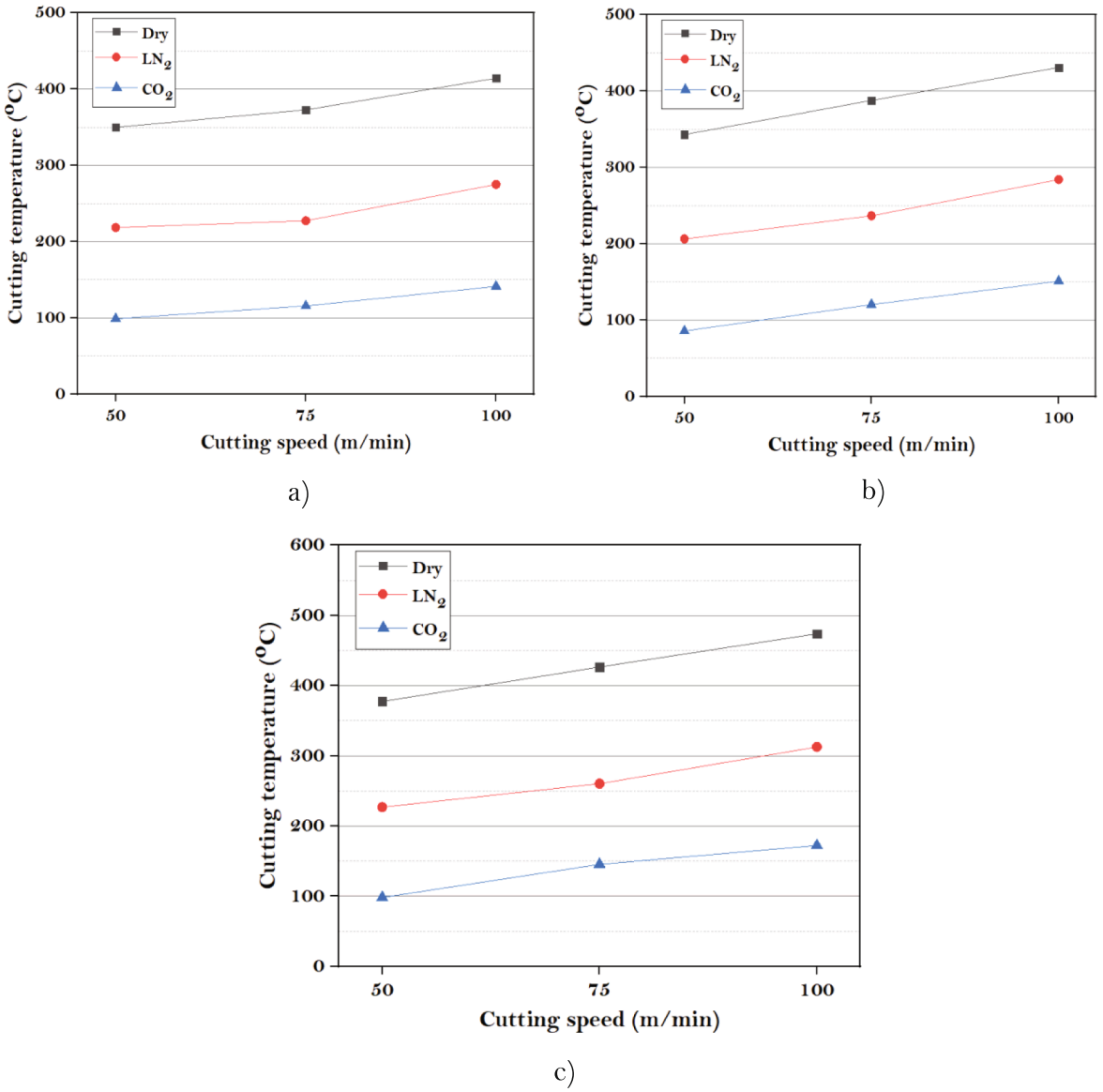

Fig. 8. Finite element results for the cutting temperature at the feed rate of a) 0.1 mm/rev, b) 0.15 mm/rev, c) 0.2 mm/rev.

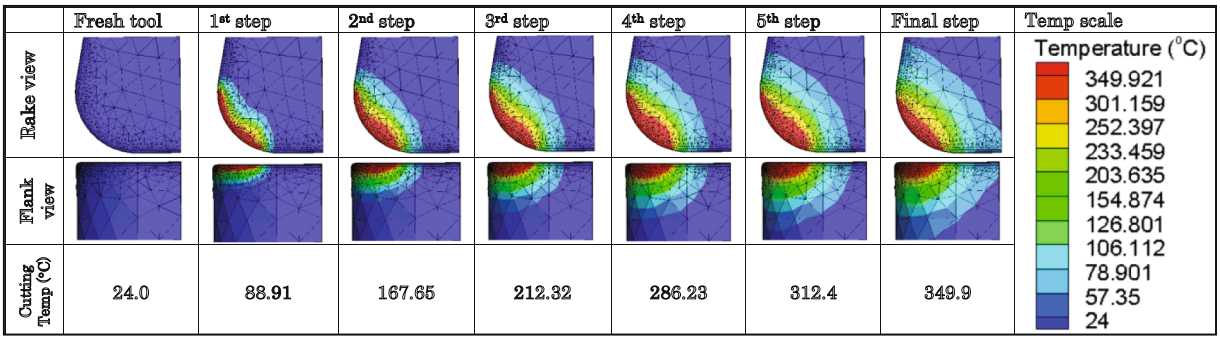

Fig. 9. Finite element steps for the cutting temperature analysis of the insert at the feed rate of 0.1 mm/rev and the cutting speed of 50 m/min in dry conditions.

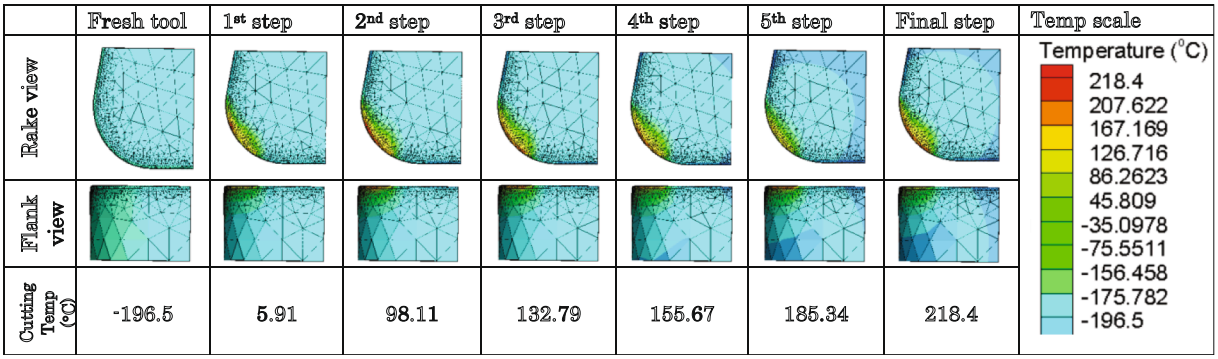

Fig. 10. Finite element steps for the cutting temperature analysis of the insert at the feed rate of 0.1 mm/rev and the cutting speed of 50 m/min in LN_2 conditions.

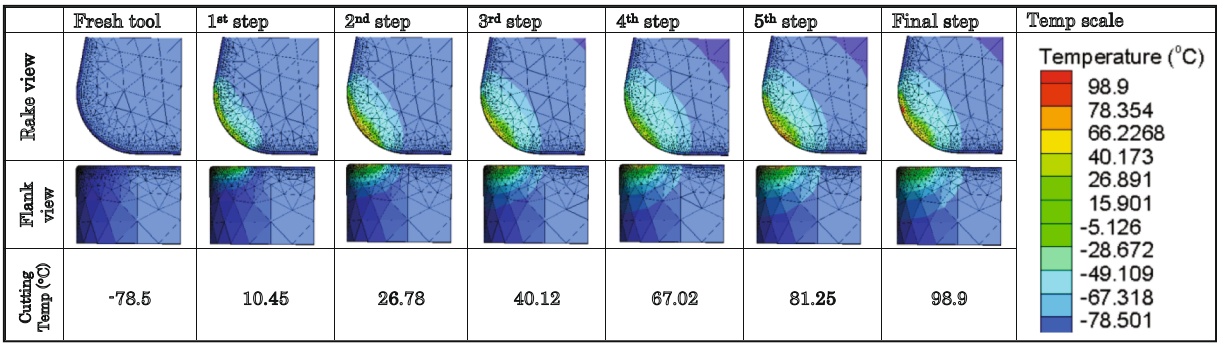

Fig. 11. Finite element steps for the cutting temperature analysis of the insert at the feed rate of 0.1 mm/rev and the cutting speed of 50 m/min in CO_2 conditions.

of the supersaturated melt. However, the adapted material in the finite element software may behave just as with the certain adapted parameters, namely JC parameters, damage constants, tensile parameters, elastic modulus, etc. The special conditions into the structure of the material cannot be defined for the material in the software. For that reason, the average deviations of 6 ~ 7% may be attributed to these circumstances. Korkmaz et al. [57] investigated the cutting force in dry turning of Nimonic 80 alloy as both experimentally and FE model and had about 6% deviations between the results. The researchers commented on the reason for the deviation that it may be attributed to both the microstructure and hardness of the workpiece material. They also stated that the deviations may be assigned to the experimental ploughing effect due to smaller depth of cut than tool nose radius. However, it is not possible to model this effect in FE software. For the cryogenic conditions, the heat transfer coefficients are assumed as constant in the FE software. Wang et al. [83] thought that the cutting and cooling process is a thermodynamically process, and thus it should be actually modelled dynamically or temperature dependent type but then Zimmerschied and Isermann [84] demonstrated that it will take so much time to solve a simple FE simulation in cryogenic conditions. That is why in the current FE study, the heat transfer coefficients and cooling temperatures of LN_2 and CO_2 cryogens were adapted as constant. This issue may be attributed to the deviations between FE model and experimental results in cryogenic conditions.

6. Conclusions

This study focuses on the dry turning and LN_2/CO_2 cooling assisted turning process of Ti6Al4V and the simulation of this process by modeling it with the finite element method. The aim of this study is to to verify the FEM simulation study with the experimental turning process and to show the estimation of the results that can be obtained from the machining process. The prominent results of this study are summarized as follows:

- The force increased with increasing cutting speed. The increase in force versus cutting speed was associated with strain hardening. Depending on the increasing cutting speed, the increase in cutting force was between 16.56% and 23.70% at 0.1 mm/rev feed, between 18.24% and 28.17% at 0.15 mm/rev feed, and between 14.23% and 26.36% at 0.20 feed mm/rev. On the other hand, an increase in feed triggered an increase in cutting force. Depending on the increase in feed, the increase in cutting force ranged from 6.72% to 23.11%.

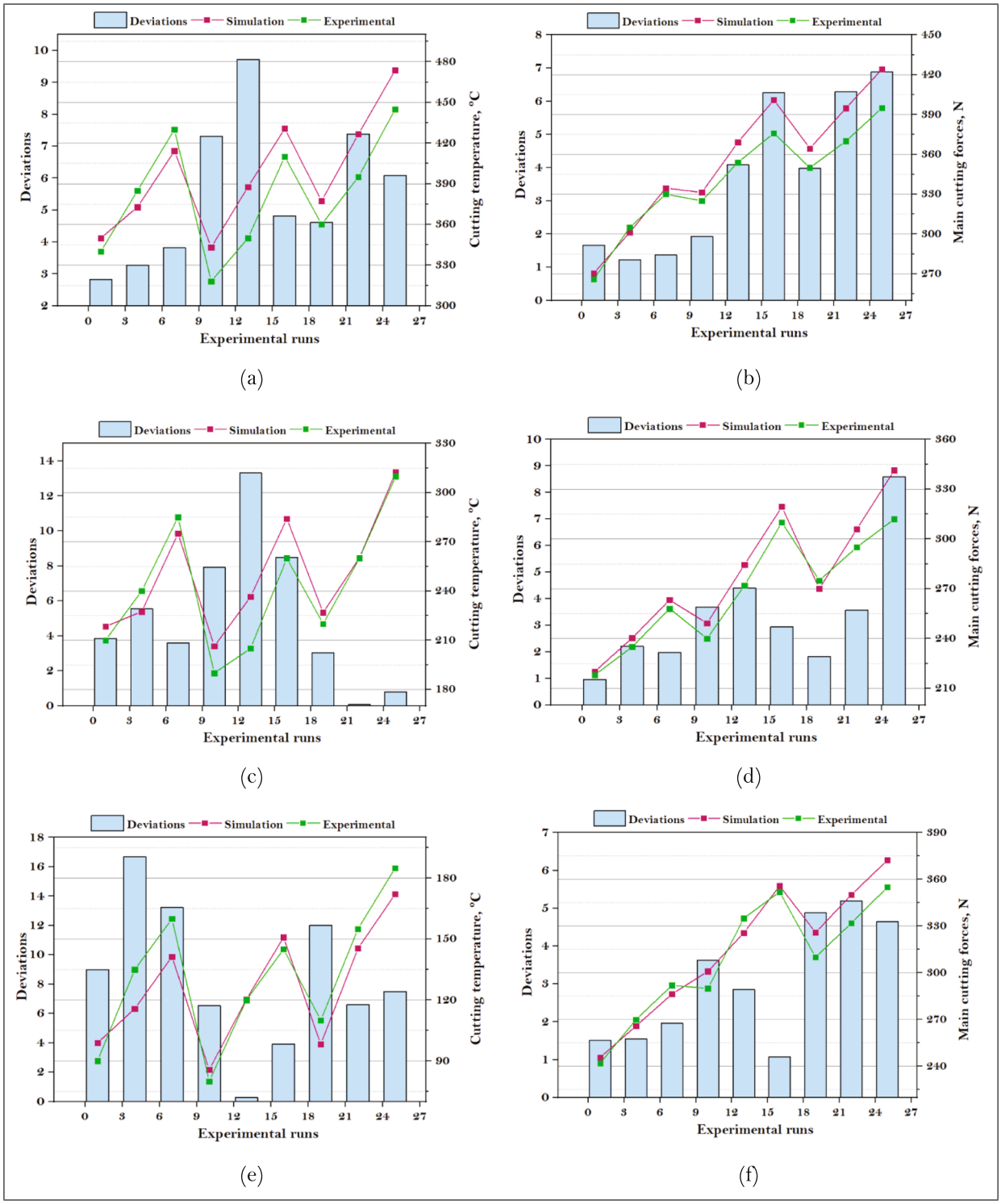

Fig. 12. Cutting temperature and cutting forces comparison of the FEM and experimental results; a-b) Dry, c-d) LN2, e-f) CO2.

- It can be determined that the cutting environment offering the lowest cutting force in each cutting parameter is LN_2 cooling followed by CO_2 and dry environment. Compared to dry cutting, 21.01% to 34.95% less cutting force can be achieved with LN_2 assisted cutting. In addition, thanks to CO_2 assisted cutting, this improvement can reach up to 14.41%.

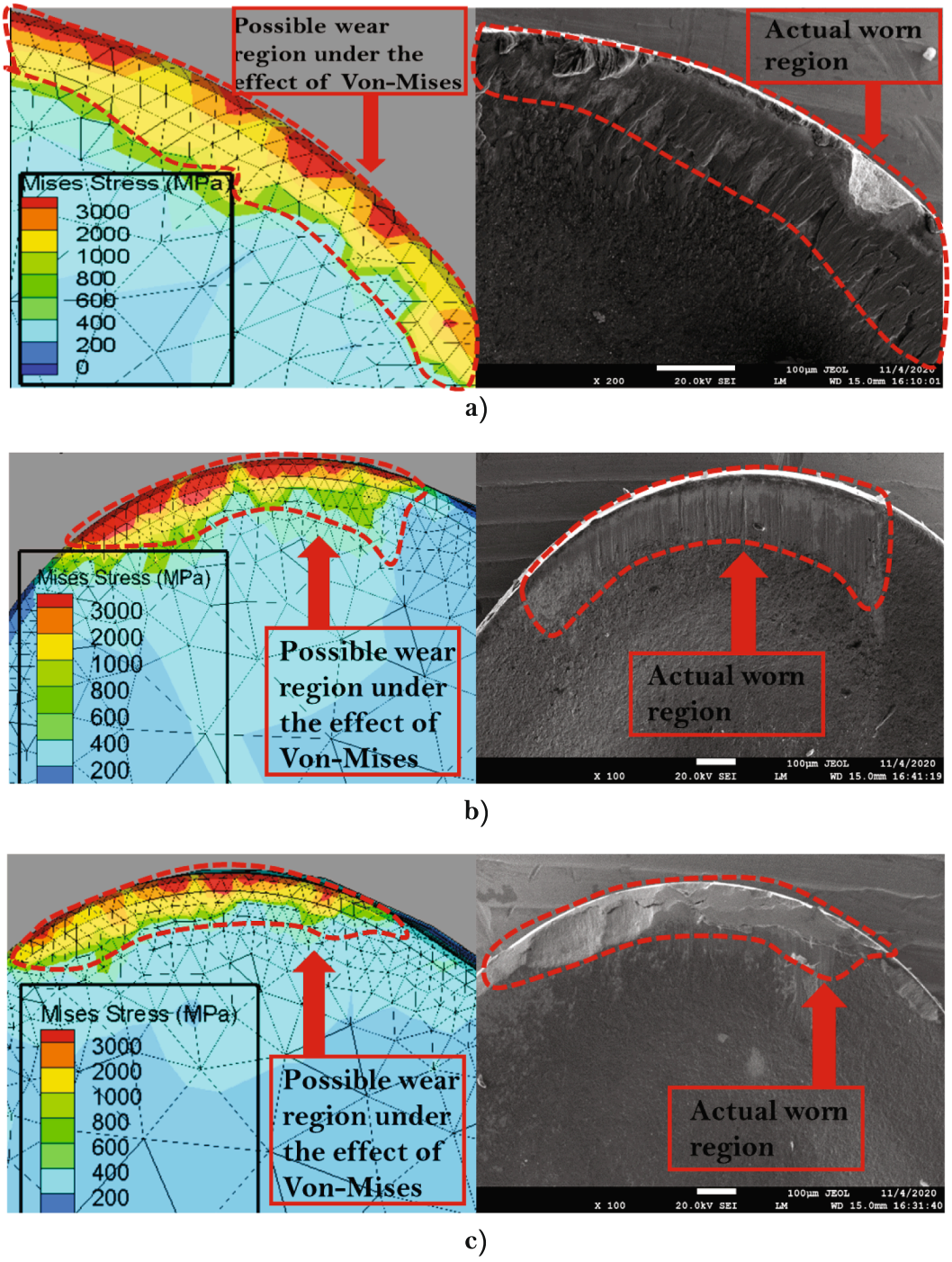

Fig. 13. The possible wear region of the inserts evaluated by FE model and the actual wear region of the cutting inserts after experimental turning for; Dry, b)LN2, and c)CO2 (Adopted and Modified: Copyrights reserved) [63].

- The upward effect of cutting speed on temperature was observed. The degree of this effect varied between 23.61% and 81.25%, depending on the feed rate and cutting environment. Feed rate was found to have a lesser effect on the cutting temperature. That is, the increase in temperature was up to 16.89% in response to an increase in feed from 0.1 to 0.2 mm/rev.
- With machining under LN_2, the cutting temperature is drastically reduced compared to machining under dry and CO_2 machining. LN_2 lowered the temperature from 58.43% to 73.53% compared to dry, and from 40.32% to 57.14% compared to CO_2. Another observation is the slowing down of the LN_2 temperature reduction rate with increasing cutting speed and feed. This is evidence that the cooling efficiency of LN_2 decreases at high cutting speeds and feed rates.

- The experimental results verified the FE model results with high accuracy. The deviations between FE modeling results and experimental results for the cutting temperature are the average of 5.54%, 5.18% and 8.42% for the dry, LN_2 and CO_2 cooling conditions, respectively. On the other hand, the deviations from FE modeling results and cutting force test results were 3.74%, 3.35%, and 3.03% under dry, LN_2 and CO2 cooling conditions, respectively.
- Although the deviation between the experimental results and the FE model results is within acceptable limits, it is not possible to mention about a complete agreement. Since the heat transfer coefficients and cooling temperatures of LN_2 and CO_2 cryogens were adapted as constant, this issue may be attributed to the deviations between FE model results and experimental results in cryogenic conditions
- This research will help to research & development centers of the machining industries , especially working on improvement of cooling technologies in the machining of biomedical materials.

CRediT authorship contribution statement

Munish Kumar Gupta: Investigation, Formal analysis, Conceptualization, Writing – review & editing. **Mehmet Erdi Korkmaz:** Investigation, Formal analysis, Conceptualization, Writing – review & editing. **Murat Sarıkaya:** Investigation, Formal analysis, Conceptualization, Writing – review & editing. **Grzegorz M. Krolczyk:** Conceptualization, Writing – review & editing, Supervision. **Mustafa Günay:** Conceptualization, Writing – review & editing, Supervision.

Declaration of Competing Interest

The authors declare that they have no known competing financial interests or personal relationships that could have appeared to influence the work reported in this paper.

Acknowledgement

The authors would like to thanks “Polısh Natıonal Agency For Academıc Exchange (NAWA) No. PPN/ULM/2020/1/00121” and National Science Centre (NCN) Project No. UMO-2020/37/K/ST8/02795 for financial supports. This work was also supported by the National Centre of Science (Decision No. 2017/25/B/ST8/00962).

References

[1] B.-A. Behrens, J. Uhe, H. Wester, T. Matthias, C. Büdenbender, FE-based Layer Design of Deposition-Welded Semi-finished Parts for the Production of Hybrid Bevel Gear, Procedia Manuf. 47 (2020) 309–314, https://doi.org/10.1016/j.promfg.2020.04.235.
[2] M.S. Nur-A-Tomal, F. Pahlevani, V. Sahajwalla, Direct transformation of waste children’s toys to high quality products using 3D printing: A waste-to-wealth and sustainable approach, J. Clean. Prod. 267 (2020), 122188, https://doi.org/10.1016/j.jclepro.2020.122188.
[3] M. Abas, L. Sayd, R. Akhtar, Q.S. Khalid, A.M. Khan, C.I. Pruncu, Optimization of machining parameters of aluminum alloy 6026–T9 under MQL-assisted turning process, J. Mater. Res. Technol. 9 (2020) 10916–10940, https://doi.org/10.1016/j.jmrt.2020.07.071.
[4] C.Y. Seif, I.S. Hage, R.F. Hamade, Utilizing the drill cutting lip to extract Johnson Cook flow stress parameters for Al6061-T6, CIRP J. Manuf. Sci. Technol. 26 (2019) 26–40, https://doi.org/10.1016/J.CIRPJ.2019.06.001.
[5] O. Pereira, J.E. Martín-Alfonso, A. Rodríguez, A. Calleja, A. Fernández-Valdivielso, L.N. López de Lacalle, Sustainability analysis of lubricant oils for minimum quantity lubrication based on their tribo-rheological performance, J. Clean. Prod. 164 (2017) 1419–1429, https://doi.org/10.1016/j.jclepro.2017.07.078.
[6] N. Khanna, P. Shah, L.N.L. de Lacalle, A. Rodríguez, O. Pereira, In pursuit of sustainable cutting fluid strategy for machining Ti-6Al-4V using life cycle analysis, Sustain. Mater. Technol. 29 (2021), e00301, https://doi.org/10.1016/j.susmat.2021.e00301.
[7] O. Pereira, G. Urbikaín, A. Rodríguez, A. Calleja, I. Ayesta, L.N. López de Lacalle, Process performance and life cycle assessment of friction drilling on dual-phase steel, J. Clean. Prod. 213 (2019) 1147–1156, https://doi.org/10.1016/j.jclepro.2018.12.250.
[8] H. Gonzalez, O. Pereira, L.N. López de Lacalle, A. Calleja, I. Ayesta, J. Muñoa, Flank-Milling of Integral Blade Rotors Made in Ti6Al4V Using Cryo CO2 and Minimum Quantity Lubrication, J. Manuf. Sci. Eng. 143 (2021) 91011.
[9] M. Mia, M.K. Gupta, G. Singh, G. Królczyk, D.Y. Pimenov, An approach to cleaner production for machining hardened steel using different cooling-lubrication conditions, J. Clean. Prod. 187 (2018) 1069–1081, https://doi.org/10.1016/j.jclepro.2018.03.279.
[10] M. Mia, M.K. Gupta, J.A. Lozano, D. Carou, D.Y. Pimenov, G. Królczyk, A.M. Khan, N.R. Dhar, Multi-objective optimization and life cycle assessment of eco-friendly cryogenic N2 assisted turning of Ti-6Al-4V, J. Clean. Prod. 210 (2019) 121–133, https://doi.org/10.1016/j.jclepro.2018.10.334.
[11] C. Xiao, H. Ding, K. Cheng, S. Chen, Design of an innovative smart turning tool with application to real-time cutting force measurement, Proc. Inst. Mech. Eng. Part B J. Eng. Manuf. 229 (3) (2015) 563–568, https://doi.org/10.1177/0954405414530907.
[12] R. Teti, D.M. D’Addona, T. Segreto, Microbial-based cutting fluids as bio-integration manufacturing solution for green and sustainable machining, CIRP J. Manuf. Sci. Technol. 32 (2021) 16–25, https://doi.org/10.1016/j.cirpj.2020.09.016.
[13] K. Orra, S.K. Choudhury, Development of flank wear model of cutting tool by using adaptive feedback linear control system on machining AISI D2 steel and AISI 4340 steel, Mech. Syst. Signal Process. 81 (2016) 475–492, https://doi.org/10.1016/j.ymssp.2016.03.011.
[14] S. Ranjith Kumar, D. Krishnaa S, K.K. Gowthamaan, D. Chandra Mouli, K. Cibi Chakravarthi, T. Balasubramanian, Development of a Re-engineered fixture to reduce operation time in a machining process, Mater. Today Proc. 37 (2021) 3179–3183.
[15] Y. Liu, J. Zhou, W. Fu, B. Zhang, F. Chang, P. Jiang, Study on the effect of cutting parameters on bamboo surface quality using response surface methodology, Measurement. 174 (2021), 109002, https://doi.org/10.1016/j.measurement.2021.109002.
[16] S. Yoo, N. Kang, Explainable artificial intelligence for manufacturing cost estimation and machining feature visualization, Expert Syst. Appl. 183 (2021), 115430, https://doi.org/10.1016/j.eswa.2021.115430.
[17] S. Shu, K. Cheng, H. Ding, S. Chen, An Innovative Method to Measure the Cutting Temperature in Process by Using an Internally Cooled Smart Cutting Tool, J. Manuf. Sci. Eng. 135 (2013). https://doi.org/10.1115/1.4025742.
[18] T. Sugihara, R. Kobayashi, T. Enomoto, Direct observations of tribological behavior in cutting with textured cutting tools, Int. J. Mach. Tools Manuf. (2021), 103726, https://doi.org/10.1016/j.ijmachtools.2021.103726.
[19] J. Zhao, Z. Liu, B. Wang, J. Hu, Y. Wan, Tool coating effects on cutting temperature during metal cutting processes: Comprehensive review and future research directions, Mech. Syst. Signal Process. 150 (2021), 107302, https://doi.org/10.1016/j.ymssp.2020.107302.

[20] W. Sawangsri, K. Cheng, An innovative approach to cutting force modelling in diamond turning and its correlation analysis with tool wear, Proc. Inst. Mech. Eng. Part B J. Eng. Manuf. 230 (3) (2016) 405–415, https://doi.org/10.1177/0954405414554020.
[21] C. Nath, T. Kurfess, Obstruction-type Chip Breakers for Controllable Chips and Improved Cooling/Lubrication During Drilling – A Feasibility Study, Procedia Manuf. 5 (2016) 375–385, https://doi.org/10.1016/j.promfg.2016.08.032.
[22] S. Li, K. Zhu, In-situ tool wear area evaluation in micro milling with considering the influence of cutting force, Mech. Syst. Signal Process. 161 (2021), 107971, https://doi.org/10.1016/j.ymssp.2021.107971.
[23] X. Wu, J. Li, Y. Jin, S. Zheng, Temperature calculation of the tool and chip in slicing process with equal-rake angle arc-tooth slice tool, Mech. Syst. Signal Process. 143 (2020), 106793, https://doi.org/10.1016/j.ymssp.2020.106793.
[24] E.L. Papazoglou, P. Karmiris-Obratański, B. Leszczyńska-Madej, A.P. Markopoulos, A study on Electrical Discharge Machining of Titanium Grade2 with experimental and theoretical analysis, Sci. Rep. 11 (2021) 8971, https://doi.org/10.1038/s41598-021-88534-8.
[25] M. Akgün, H. Demir, Optimization and finite element modelling of tool wear in milling of Inconel 625 superalloy, J. Polytech. 24 (2021) 391–400, https://doi.org/10.2339/politeknik.706605.
[26] T. Zhou, L. He, Z. Zou, F. Du, J. Wu, P. Tian, Three-dimensional turning force prediction based on hybrid finite element and predictive machining theory considering edge radius and nose radius, J. Manuf. Process. 58 (2020) 1304–1317, https://doi.org/10.1016/j.jmapro.2020.09.034.
[27] M. Lotfi, S. Amini, S.A. Sajjady, Development of a friction model based on oblique cutting theory, Int. J. Mech. Sci. 160 (2019) 241–254, https://doi.org/10.1016/j.ijmecsci.2019.06.038.
[28] C.S. Kumar, P. Zeman, T. Polcar, A 2D finite element approach for predicting the machining performance of nanolayered TiAlCrN coating on WC-Co cutting tool during dry turning of AISI 1045 steel, Ceram. Int. 46 (2020) 25073–25088, https://doi.org/10.1016/j.ceramint.2020.06.294.
[29] J. Yang, X. Wang, M. Kang, Finite element simulation of surface roughness in diamond turning of spherical surfaces, J. Manuf. Process. 31 (2018) 768–775, https://doi.org/10.1016/J.JMAPRO.2018.01.006.
[30] V. Vijayaraghavan, A. Garg, L. Gao, R. Vijayaraghavan, G. Lu, A finite element based data analytics approach for modeling turning process of Inconel 718 alloys, J. Clean. Prod. 137 (2016) 1619–1627, https://doi.org/10.1016/j.jclepro.2016.04.010.
[31] A.K. Parida, K. Maity, FEM analysis and experimental investigation of force and chip formation on hot turning of Inconel 625, Def. Technol. 15 (6) (2019) 853–860, https://doi.org/10.1016/j.dt.2019.04.012.
[32] S. Schindler, M. Zimmermann, J.C. Aurich, P. Steinmann, Thermo-elastic deformations of the workpiece when dry turning aluminum alloys - A finite element model to predict thermal effects in the workpiece, CIRP J. Manuf. Sci. Technol. 7 (2014) 233–245, https://doi.org/10.1016/j.cirpj.2014.04.006.
[33] M. Sadeghifar, M. Javidikia, V. Songmene, M. Jahazi, Finite element simulation-based predictive regression modeling and optimum solution for grain size in machining of Ti6Al4V alloy: Influence of tool geometry and cutting conditions, Simul. Model. Pract. Theory. 104 (2020), 102141, https://doi.org/10.1016/j.simpat.2020.102141.
[34] S. Razanica, A. Malakizadi, R. Larsson, S. Cedergren, B.L. Josefson, FE modeling and simulation of machining Alloy 718 based on ductile continuum damage, Int. J. Mech. Sci. 171 (2020) 105375, https://doi.org/10.1016/j.ijmecsci.2019.105375.
[35] S.K. Mishra, S. Ghosh, S. Aravindan, Performance of laser processed carbide tools for machining of Ti6Al4V alloys: A combined study on experimental and finite element analysis, Precis. Eng. 56 (2019) 370–385, https://doi.org/10.1016/j.precisioneng.2019.01.006.
[36] A.K. Parida, K. Maity, Effect of nose radius on forces, and process parameters in hot machining of Inconel 718 using finite element analysis, Eng. Sci. Technol. an Int. J. 20 (2) (2017) 687–693, https://doi.org/10.1016/j.jestch.2016.10.006.
[37] M. Du, Z. Cheng, S. Wang, Finite element modeling of friction at the tool-chip-workpiece interface in high speed machining of Ti6Al4V, Int. J. Mech. Sci. 163 (2019), 105100, https://doi.org/10.1016/j.ijmecsci.2019.105100.
[38] F.A.V. da Silva, J.C. Outeiro, Machining simulation of Inconel 718 using Lagrangian and Coupled Eulerian-Lagrangian approaches, Procedia CIRP. 102 (2021) 453–458, https://doi.org/10.1016/j.procir.2021.09.077.
[39] V. Veeranaath, Experimental Investigation of Process Parameters in Orthogonal Machining of Ti6Al4V with TiC Coated PCBN Inserts – A Finite Element Analysis, Mater. Today Proc. 5 (2018) 19547–19554, https://doi.org/10.1016/j.matpr.2018.06.316.
[40] P. Niesłony, W. Grzesik, K. Jarosz, P. Laskowski, FEM-based optimization of machining operations of aerospace parts made of Inconel 718 superalloy, Procedia CIRP. 77 (2018) 570–573, https://doi.org/10.1016/j.procir.2018.08.220.
[41] F.J. Amigo, G. Urbikain, O. Pereira, P. Fernández-Lucio, A. Fernández-Valdivielso, L.N.L. de Lacalle, Combination of high feed turning with cryogenic cooling on Haynes 263 and Inconel 718 superalloys, J. Manuf. Process. 58 (2020) 208–222, https://doi.org/10.1016/j.jmapro.2020.08.029.
[42] O. Pereira, P. Català, A. Rodríguez, T. Ostra, J. Vivancos, A. Rivero, L.N. López-de-Lacalle, The Use of Hybrid CO2+MQL in Machining Operations, Procedia Eng. 132 (2015) 492–499, https://doi.org/10.1016/j.proeng.2015.12.524.
[43] O. Pereira, A. Rodríguez, A.I. Fernández-Abia, J. Barreiro, L.N. López de Lacalle, Cryogenic and minimum quantity lubrication for an eco-efficiency turning of AISI 304, J. Clean. Prod. 139 (2016) 440–449, https://doi.org/10.1016/j.jclepro.2016.08.030.
[44] O. Pereira, G. Urbikain, A. Rodríguez, A. Fernández-Valdivielso, A. Calleja, I. Ayesta, L.N.L. de Lacalle, Internal cryolubrication approach for Inconel 718 milling, Procedia Manuf. 13 (2017) 89–93, https://doi.org/10.1016/j.promfg.2017.09.013.
[45] O. Pereira, A. Rodríguez, A. Fernández-Valdivielso, J. Barreiro, A.I. Fernández-Abia, L.N. López-de-Lacalle, Cryogenic Hard Turning of ASP23 Steel Using Carbon Dioxide, Procedia Eng. 132 (2015) 486–491, https://doi.org/10.1016/j.proeng.2015.12.523.
[46] J.-H. Urrea-Quintero, M. Marino, H. Hernandez, S. Ochoa, Multiscale modeling of a free-radical emulsion polymerization process: Numerical approximation by the Finite Element Method, Comput. Chem. Eng. 140 (2020), 106974, https://doi.org/10.1016/j.compchemeng.2020.106974.
[47] K.O. Coelho, P.R.B. Devloo, S.M. Gomes, Error estimates for the Scaled Boundary Finite Element Method, Comput. Methods Appl. Mech. Eng. 379 (2021), 113765, https://doi.org/10.1016/j.cma.2021.113765.
[48] N. Yaşar, Thrust force modelling and surface roughness optimization in drilling of AA-7075: FEM and GRA, J. Mech. Sci. Technol. 33 (10) (2019) 4771–4781, https://doi.org/10.1007/s12206-019-0918-5.
[49] K. Gok, Development of three-dimensional finite element model to calculate the turning processing parameters in turning operations, Measurement. 75 (2015) 57–68, https://doi.org/10.1016/J.MEASUREMENT.2015.07.034.
[50] R.L. Thomes, F.C.M. Menandro, Polygonal finite element: A comparison of the stiffness matrix integration methods, Appl. Math. Comput. 375 (2020), 125089, https://doi.org/10.1016/j.amc.2020.125089.
[51] V. Mercuri, G. Balduzzi, D. Asprone, F. Auricchio, Structural analysis of non-prismatic beams: Critical issues, accurate stress recovery, and analytical definition of the Finite Element (FE) stiffness matrix, Eng. Struct. 213 (2020), 110252, https://doi.org/10.1016/j.engstruct.2020.110252.
[52] A. Chikhi, M. Djermane, Dynamic buckling of cylindrical storage tanks during earthquake excitations, MOJ Civ. Eng. 3 (2017) 227-232. https://doi.org/10.15406/mojce.2017.03.00058.
[53] S. Savidis, D. Aubram, F. Rackwitz, Arbitrary Lagrangian-Eulerian Finite Element Formulation for Geotechnical Construction Processes, J. Theor. Appl. Mech. 38 (2008) 165–194.
[54] W. Grzesik, Chapter Nine - Heat in Metal Cutting, in: W.B.T.-A.M.P. of M.M. (Second E. Grzesik (Ed.), Adv. Mach. Process. Met. Mater. (Second Ed., Elsevier, 2017: pp. 163–182. https://doi.org/https://doi.org/10.1016/B978-0-444-63711-6.00009-0.
[55] X. Xu, J. Zhang, J. Outeiro, B. Xu, W. Zhao, Multiscale simulation of grain refinement induced by dynamic recrystallization of Ti6Al4V alloy during high speed machining, J. Mater. Process. Technol. 286 (2020), 116834, https://doi.org/10.1016/j.jmatprotec.2020.116834.
[56] X. Xie, G. Kang, Q. Kan, C. Yu, Phase-field theory based finite element simulation on thermo-mechanical cyclic deformation of polycrystalline super-elastic NiTi shape memory alloy, Comput. Mater. Sci. 184 (2020), 109899, https://doi.org/10.1016/j.commatsci.2020.109899.
[57] M.E. Korkmaz, N. Yaşar, M. Günay, Numerical and experimental investigation of cutting forces in turning of Nimonic 80A superalloy, Eng. Sci. Technol. an Int. J. 23 (3) (2020) 664–673, https://doi.org/10.1016/j.jestch.2020.02.001.
[58] S.K. Josyula, S.K.R. Narala, Study of TiC particle distribution in Al-MMCs using finite element modeling, Int. J. Mech. Sci. 141 (2018) 341–358, https://doi.org/10.1016/j.ijmecsci.2018.04.004.

[59] M.K. Gupta, Q. Song, Z. Liu, M. Sarikaya, M. Jamil, M. Mia, N. Khanna, G.M. Krolczyk, Experimental characterisation of the performance of hybrid cryo-lubrication assisted turning of Ti–6Al–4V alloy, Tribol. Int. 153 (2021), 106582, https://doi.org/10.1016/j.triboint.2020.106582.
[60] S. Canovic, B. Ljungberg, C. Björmander, M. Halvarsson, CVD TiC/alumina and TiN/alumina multilayer coatings grown on sapphire single crystals, Int. J. Refract. Met. Hard Mater. 28 (2010) 163–173, https://doi.org/10.1016/j.ijrmhm.2009.08.001.
[61] M. Akgün, H. Demir, Optimization of Cutting Parameters Affecting Surface Roughness in Turning of Inconel 625 Superalloy by Cryogenically Treated Tungsten Carbide Inserts, SN Appl. Sci. 3 (2021) 277, https://doi.org/10.1007/s42452-021-04303-2.
[62] H. Kaya, O. Uluer, E. Kocaoğlu, V. Kirmaci, Experimental analysis of cooling and heating performance of serial and parallel connected counter-flow Ranquee-Hilsch vortex tube systems using carbon dioxide as a working fluid, Int. J. Refrig. 106 (2019) 297–307, https://doi.org/10.1016/j.ijrefrig.2019.07.004.
[63] M.K. Gupta, Q. Song, Z. Liu, M. Sarikaya, M. Mia, M. Jamil, A.K. Singla, A. Bansal, D.Y. Pimenov, M. Kuntoğlu, Tribological performance based machinability investigations in cryogenic cooling assisted turning of α-β titanium Alloy, Tribol. Int. 160 (2021), 107032, https://doi.org/10.1016/j.triboint.2021.107032.
[64] T. Özel, The influence of friction models on finite element simulations of machining, Int. J. Mach. Tools Manuf. 46 (2006) 518–530, https://doi.org/10.1016/j.ijmachtools.2005.07.001.
[65] Y. Yang, L. Jin, J. Zhu, J. Kong, L. Li, Study on Cutting Force, Cutting Temperature and Machining Residual Stress in Precision Turning of Pure Iron with Different Grain Sizes, Chinese J. Mech. Eng. 33 (2020) 53, https://doi.org/10.1186/s10033-020-00471-1.
[66] B.N. Pathak, K.L. Sahoo, M. Mishra, Effect of Machining Parameters on Cutting Forces and Surface Roughness in Al-(1–2) Fe-1V-1Si Alloys, Mater. Manuf. Process. 28 (4) (2013) 463–469, https://doi.org/10.1080/10426914.2013.763952.
[67] U. Şeker, A. Kurt, İ. Çiftçi, The effect of feed rate on the cutting forces when machining with linear motion, J. Mater. Process. Technol. 146 (2004) 403–407, https://doi.org/10.1016/j.jmatprotec.2003.12.001.
[68] S. Ravi, M. Pradeep Kumar, Experimental investigations on cryogenic cooling by liquid nitrogen in the end milling of hardened steel, Cryogenics (Guildf) 51 (9) (2011) 509–515, https://doi.org/10.1016/j.cryogenics.2011.06.006.
[69] J. Hou, W. Zhou, H. Duan, G. Yang, H. Xu, N. Zhao, Influence of cutting speed on cutting force, flank temperature, and tool wear in end milling of Ti-6Al-4V alloy, Int. J. Adv. Manuf. Technol. 70 (9-12) (2014) 1835–1845, https://doi.org/10.1007/s00170-013-5433-8.
[70] Q.i. Shi, L. Li, N. He, W. Zhao, X. Liu, Experimental study in high speed milling of titanium alloy TC21, Int. J. Adv. Manuf. Technol. 64 (1-4) (2013) 49–54, https://doi.org/10.1007/s00170-012-3997-3.
[71] D.M. Kim, D.Y. Kim, N. Banerjee, H.W. Park, Predictive modeling for the cryogenic cooling condition of the hard turning process, Int. J. Adv. Manuf. Technol. 99 (9-12) (2018) 2877–2891, https://doi.org/10.1007/s00170-018-2660-z.
[72] F. Pusavec, A. Deshpande, S. Yang, R. M'Saoubi, J. Kopac, O.W. Dillon, I.S. Jawahir, Sustainable machining of high temperature Nickel alloy – Inconel 718: part 1 – predictive performance models, J. Clean. Prod. 81 (2014) 255–269, https://doi.org/10.1016/j.jclepro.2014.06.040.
[73] S.Y. Hong, Y. Ding, W.-C. Jeong, Friction and cutting forces in cryogenic machining of Ti-6Al-4V, Int. J. Mach. Tools Manuf. 41 (15) (2001) 2271–2285, https://doi.org/10.1016/S0890-6955(01)00029-3.
[74] P. Singh, H. Pungotra, N.S. Kalsi, On the Complexities in Machining Titanium Alloys, in: D.K. Mandal, C.S. Syan (Eds.), CAD/CAM, Robot. Factories Futur, Springer India, New Delhi, 2016, pp. 499–507.
[75] A. Pramanik, Problems and solutions in machining of titanium alloys, Int. J. Adv. Manuf. Technol. 70 (5-8) (2014) 919–928, https://doi.org/10.1007/s00170-013-5326-x.
[76] Kiprawi, Mohammad Ashaari, Yassin, Abdullah, Syed Shazali, Syed Tarmizi, Islam, M. Shahidul, Mohd Said, Mohd Azrin, Study of Cutting Edge Temperature and Cutting Force of End Mill Tool in High Speed Machining, MATEC Web Conf. 87 (2017) 2030. https://doi.org/10.1051/matecconf/20178702030.
[77] H.-B. He, H.-Y. Li, J. Yang, X.-Y. Zhang, Q.-B. Yue, X. Jiang, S.-k. Lyu, A study on major factors influencing dry cutting temperature of AISI 304 stainless steel, Int. J. Precis. Eng. Manuf. 18 (10) (2017) 1387–1392, https://doi.org/10.1007/s12541-017-0165-6.
[78] T. Özel, M. Sima, A.K. Srivastava, B. Kaftanoglu, Investigations on the effects of multi-layered coated inserts in machining Ti–6Al–4V alloy with experiments and finite element simulations, CIRP Ann. 59 (2010) 77–82, https://doi.org/10.1016/j.cirp.2010.03.055.
[79] Y. Guo, G. Quan, M. Celikin, L. Ren, Y. Zhan, L. Fan, H. Pan, Effect of heat treatment on the microstructure and mechanical properties of AZ80M magnesium alloy fabricated by wire arc additive manufacturing, J. Magnes Alloy (2021), https://doi.org/10.1016/j.jma.2021.04.006.
[80] Q. Zheng, T. Furushima, Evaluation of high-temperature tensile behavior for metal foils by a novel resistance heating assisted tensile testing system using samples with optimized structures, J. Mater. Sci. Technol. 94 (2021) 216–229, https://doi.org/10.1016/j.jmst.2021.03.061.
[81] M. Abdel-Salam, S. El-Hadad, W. Khalifa, Effects of microstructure and alloy composition on hydroxyapatite precipitation on alkaline treated α/β titanium alloys, Mater. Sci. Eng. C. 104 (2019), 109974, https://doi.org/10.1016/j.msec.2019.109974.
[82] B. Fu, H. Wang, C. Zou, Z. Wei, The influence of Zr content on microstructure and precipitation of silicide in as-cast near α titanium alloys, Mater. Charact. 99 (2015) 17–24, https://doi.org/10.1016/j.matchar.2014.09.015.
[83] C. Wang, H. Ding, H. Wang, Thermodynamic Model and Dynamic Temperature Compensation in Positive-Pressure-Based Sonic Nozzle Gas Flow Standard, IEEE Trans. Instrum. Meas. 62 (5) (2013) 1154–1165, https://doi.org/10.1109/TIM.2012.2234599.
[84] R. Zimmerschied, R. Isermann, Nonlinear time constant estimation and dynamic compensation of temperature sensors, Control Eng, Pract. - Control ENG Pract. 18 (3) (2010) 300–310, https://doi.org/10.1016/j.conengprac.2009.11.008.